Spectromicroscopy study of the dynamics of submonolayer Pd on a polycrystalline Ni surface

A. W. Potts and G. R. Morrison
Department of Physics, King's College, Strand, London WC2R 2LS, United Kingdom

L. Gregoratti, M. Kiskinova, and A. Locatelli
Sincrotrone Trieste, Area Science Park, SS14-Km163.5, 34012 Basovizza, Trieste, Italy

(Received 31 May 2002; revised manuscript received 18 November 2002; published 29 January 2003)

The lateral distribution of submonolayer Pd deposited at room temperature on the surface of a polycrystalline Ni sample has been studied with scanning photoelectron microscopy (SPEM). The Ni sample consisted of differently oriented crystal grains, as evidenced by low-energy electron microscopy and micro-low-energy electron diffraction measurements and by SPEM Ni $3p$ maps showing surface topography. The elemental contrast of the SPEM Pd $3d$ images have revealed that the different grains of the polycrystalline surface show different activity, resulting in differences in the local Pd concentrations. The chemical state of Pd was well described by the Pd $3d_{5/2}$ spectra. They consisted of two components interpreted in terms of adsorbed Pd species (Pd $3d_{5/2}$ binding energy of 336.0 eV) and Pd embedded in the Ni a surface lattice, forming surface Pd_xNi_y alloy (Pd $3d_{5/2}$ binding energy at 335.5 eV). Chemical imaging in terms of these Pd $3d_{5/2}$ components confirmed that the ability of Pd to alloy or form clusters also depends on the individual structure of the grains on the polycrystalline Ni surface.

DOI: 10.1103/PhysRevB.67.045411 PACS number(s): 68.37.Xy, 61.66.Dk, 68.35.Fx, 68.35.Ct

I. INTRODUCTION

The study of binary metallic systems is important because of their many technological applications, e.g., in catalysis and magnetic recording.[1] The behavior of the system components at the surface is typically different from that in the bulk. This has motivated a series of studies to characterize structurally and chemically the interface between metallic species. These studies have demonstrated the great variety of phenomena which may occur when one species is deposited on another. In particular phenomena such as surface segregation, diffusion, nucleation, and alloying have been observed. Alloying has been the subject of many studies during recent years, and it has been found that elements which do not form alloys in the bulk phase can do so when reacting on a surface.[2,3] Detailed chemical and geometrical information on surface layers may be obtained by surface core-level spectroscopy since core-level binding energies are sensitive to the environment of the emitting atoms. The typical core-level energy shifts between elements involved in surface or bulk alloy formation are of the order of a few hundred meV, as found for several bimetallic systems.[4,5] X-ray photoelectron spectroscopy (XPS) performed with sufficient energy resolution is thus a suitable technique for the study of surface alloying.

When alloyed at high temperatures Pd and Ni form a solid solution over the whole range of composition. Scanning tunneling microscopy (STM), low-energy ion scattering spectroscopy (LEIS), XPS, and Auger electron spectroscopy (AES) measurements have provided evidence for Pd segregation on the outermost layers of the bulk alloys.[6–9] Previous photoemission studies of bulk alloys have shown clear evidence for the presence of surface and subsurface Pd species. The annealed bulk alloy corresponds to the classical thermodynamical limit but simple deposition may produce a metastable surface or interface alloy since the surface temperature will normally be too low for thermodynamic equilibrium to be achieved. To our knowledge the initial stages of the reaction between Pd atoms deposited over a Ni surface have been studied only for the Ni(110) surface by means of STM.[7,9] From these studies it was found that at room temperature (RT) the Pd atoms landing on a terrace of a (110) Ni face can aggregate to form stable clusters on a nanometer scale. These will grow preferentially along the easy direction of diffusion, the [110] direction, resulting in Pd island formation. Apart from the growth of Pd islands the STM images from the Ni(110) surface show the presence of poorly defined regions near steps between Ni terraces. In these regions Pd and Ni atoms are assumed to exchange their position, forming an ordered surface alloy even at room temperature.[9] The atomic model proposed by Abel *et al.*[7] involves a relaxation of the topmost Ni layer to accommodate the strain induced by the 10% relative mismatch in crystal spacing between Pd and Ni. For this reason substitution should be easier on the upper terraces near to surface steps and kinks of single-crystal planes. Atomic substitution is considered as the preferred way to arrange a surface alloy on a (110) fcc substrate, as also observed for the Au/Ni interface.[3,10] Several other works also indicate that the formation of a surface alloy should be quite general, occurring even at RT for metal-on-metal systems.[3,11] In this investigation we have linked photoemission spectroscopy with the imaging capabilities of the scanning photoemission microscope (SPEM). This has allowed the composition of individual grains of a polycrystalline surface to be probed with submicrometer lateral resolution. Effects have been identified in the interaction of a submonolayer Pd film deposited on a polycrystalline Ni substrate that results specifically from the different grain structures coexisting in the polycrystalline environment.

II. EXPERIMENT

The spectromicroscopy measurements reported in this work were performed with the SPEM of the ESCA micros-

copy beamline at the Elettra Synchrotron Light Source. The photon beam was demagnified to a microspot of ≈ 150 nm diameter by means of a Fresnel zone plate, and the photoelectrons produced were collected by a hemispherical electron energy analyzer with a multichannel detector. The preparation of the surface was performed in a UHV chamber connected to the SPEM chamber. A detailed description of the microscope and associated facilities can be found in Ref. 12.

Two-dimensional maps of the sample surface have been obtained by scanning the sample with respect to the focused x-ray beam and collecting the photoelectrons with a selected kinetic energy at each scan step. Spectra have been acquired from small regions of a size comparable with the x-ray microspot. The electron take-off angle was 20° to the sample surface, which enhanced the surface contribution in the data collected. A photon energy of 500 eV was used for all the photoemission measurements. Using the atomic cross sections and the escape depth of photoelectrons, the depth of the sample probed by the apparatus can be established. For the experimental geometry used it is limited to the top five to seven atomic layers, with $\approx 70\%$ of the signal coming from the top two layers.

The multichannel electron detector of the electron analyzer was used to generate maps of the different chemical states of the Pd atoms on the Ni surface. The electron kinetic energies and analyzer pass energies are chosen so that the different channels of the detector receive photoelectron signal from different energy positions across the Pd $3d_{5/2}$ core-level components simultaneously. This avoids any misalignment of the maps corresponding to these energies (or channels), which would introduce artifacts in images when intensities are ratioed or subtracted to highlight changes.

The Ni sample was prepared from 99.98% pure commercial foil, 0.25 mm thick, and was compressed against a polished Si wafer using a hydraulic press to achieve a flat surface. The sample was cleaned under UHV conditions (2×10^{-10} mbar base pressure) by several cycles involving heating at 900 K in a 1×10^{-6} mbar oxygen atmosphere, followed by 500 eV Ar^+ bombardment and annealing to 1100 K in order to produce a smooth C- and O-free surface, as measured with AES. The Pd depositions were performed from a 99.99% pure Pd rod with a commercial electron bombardment water-cooled evaporator. The amount of deposited Pd was 4×10^{14} atoms cm^{-2}. Expressed in monolayers (ML), defined as the number of Pd atoms per surface Ni atom, the deposited amount is <0.5 ML. Low-energy electron microscopy (LEEM) and micro-low-energy electron diffraction (μ-LEED) images were acquired by using an Elmitec LEEM 3 low-energy electron microscope. A detailed description of this instrument can be found in Ref. 13. Using the lenses in the imaging column, the instrument can be quickly switched from LEEM to μ-LEED mode. Inserting a circular aperture into the illuminating beam at the beam separator allows μ-LEED analysis to be performed. The data presented in this work were obtained using a 100 μm aperture, thus illuminating a 5 μm spot on the sample.

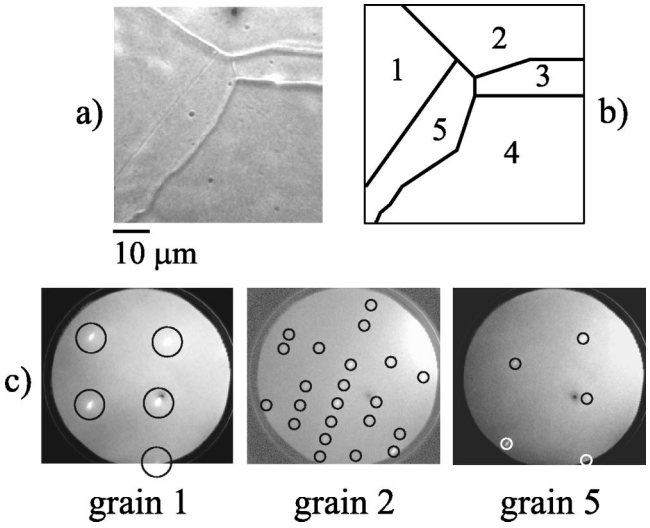

FIG. 1. (a) LEEM image of a 64×64 μm^2 area of the clean Ni polycrystalline sample where grain boundaries are clearly visible. The LEEM image was acquired by selecting electrons from the (0,0) diffraction spot at 3.5 eV. The black spots visible in the picture are damaged zones of the phosphor screen. (b) Sketch of the Ni grains in the explored area labeled from 1 to 5. (c) μ-LEED patterns, obtained by collecting the signal from a 3–4 μm^2 region inside grains 1, 2, and 5. Since some spots have poor contrast and are difficult to see, they have been ringed for clarity.

III. RESULTS

A. LEEM and μ-LEED of the polycrystalline Ni sample

Figure 1(a) shows an area of the clean polycrystalline sample obtained with a LEEM. The continuous lines visible in the picture are boundaries between the different Ni grains labeled in Fig. 1(b). The μ-LEED patterns acquired on the different grains are shown in Fig. 1(c). The quality of the patterns is not good enough for a reliable interpretation of the surface structures to be made. However, they do indicate that the different grain surfaces observed have different crystal orientations and enable suggestions to be made as to the likely surface structures. Grain 1 shows four spots at the corners of a square. It is therefore reasonable to suggest that its orientation corresponds to a (100) surface. The LEED pattern for grain 2 contains several lines of spots alternately shifted with respect to one another. The orientation in this case suggests a (110) face with possible reconstructions. The LEED patterns recorded on crystals 3 and 4 were very poor and did not show any ordered structure. This is an important indication of the roughness of the surface that will help the interpretation of the photoemission data. Finally the pattern observed for grain 5 suggests a hexagonal (111) face. These measurements show that the region of the sample selected is formed by several planes with different orientations and characterized by different levels of roughness. As will be shown later, this interpretation agrees with the photoemission spectra and images acquired with SPEM. These qualitative assignments of the micro-LEED spots were carried out by comparison with the spot positions observed in the LEED pattern from a (110) face of a reference W crystal.

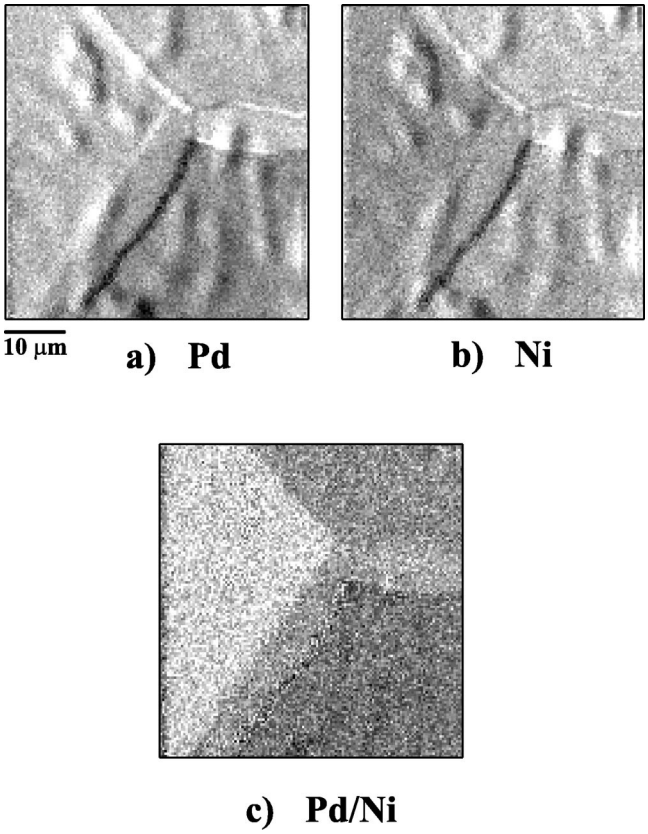

FIG. 2. (a) and (b): Pd $3d_{5/2}$ and Ni $3p$ chemical maps of the Ni polycrystalline sample. The two pictures are quite similar because the major source of contrast is topography. Lines are interpreted as topographical evidence of grain boundaries. Other features are simply mesoscopic topography left from the sample preparation procedure. The area scanned is 64×64 μm^2. Picture (c) is the ratio of images (a) and (b) on a pixel-by-pixel basis. This procedure eliminates any topographic contribution; the result represents the proportion of Pd present in the Ni surface layers.

B. SPEM of the polycrystalline Ni sample with a submonolayer of Pd

Figure 2 shows SPEM images of the same area of the clean Ni surface, characterized by LEEM and μ-LEED (Fig. 1), taken after deposition of 4×10^{14} atoms cm^{-2} of Pd. These images were recorded with 500 nm scan steps. The raw SPEM images [Fig. 2(a) and 2(b)] correspond to the sum of the signals from all the detector channels covering the energy windows of the Pd $3d$ (a) and Ni $3p$ (b) photoelectron emission, respectively. They look very similar, since the main source of contrast is the topography, which is strongly enhanced by the 20° take-off angle used in the SPEM. However, concentration contrast, due to the presence of different amounts of Pd on the different grains, is also visible even in the raw images. The bottom image [Fig. 2(c)] is obtained by division of the raw Pd image by the raw Ni image on a pixel-by-pixel basis. This procedure removes features due to surface topography from the images, leaving only elemental information. The substantial variations of elemental Pd concentration between the different grains (identified in Fig. 1) produce clear contrast in the processed Pd image in Fig. 2(c). The signal, which appears to be uniform inside each grain, is a maximum on grain 1 where the surface is Pd rich and lower on the other planes, but with different intensities. Assuming that the average surface concentration of the imaged area is 4×10^{14} atoms cm^{-2}, simple calculations based on the difference in the gray levels give the relative surface concentrations of Pd and hence the following local concentrations for the different grains: $\approx4.6\times10^{14}$ atoms cm^{-2} for grain 1 [0.35 ML assuming a (110) surface], $\approx4\times10^{14}$ atoms cm^{-2} for grain 5 [0.25 ML assuming a (111) surface], $\approx3.8\times10^{14}$ atoms cm^{-2} for grain 2 [0.38 ML assuming a (110) surface], and $\approx3.5\times10^{14}$ atoms cm^{-2} for disordered grain 4. For surfaces where a surface structure has been suggested by the μ-LEED measurements, the density of Ni atoms has been assumed and the surface Pd density is normalized in terms of the Ni density to give the surface coverage in ML for the suggested surface structures. No particular feature is observed on the boundaries between the crystal grains. As will be shown below, the analysis of the images formed in terms of the signal from selected detector channels produces more detailed maps, showing not only the elemental distributions, but also contrast resulting from the different chemical states of the adsorbed Pd.

In contrast to the Pd images the inhomogeneous distribution of Pd has negligible effect on the contrast between the different grains of the Ni $3p$ images. In fact a nearly uniform Ni map without significant contrast was obtained by applying the procedure described above for removal of topographical effects from the Ni $3p$ images acquired after the Pd deposition. In this case the images were divided by the Ni $3p$ maps of the same area obtained before Pd deposition. The lack of contrast in the Ni $3p$ maps is not unexpected, because its origin is the attenuation of the Ni $3p$ emission by the deposited Pd film. In the present case the difference in the Pd concentration between the grains is of the order of or less than 10^{14} atoms cm^{-2}, i.e., $\leqslant0.1$ ML. This apparently leads to a negligibly small difference in the attenuation effect of Pd, which is confirmed by the Ni $3p$ spectra taken on the different grains (see Fig. 3). The low Ni $3p$ photoionization cross section and the higher escape depth of the Ni $3p$ photoelectrons also contribute to the negligible effect that the inhomogeneous Pd distribution has on the Ni $3p$ signal.

The Ni $3p$ photoemission spectra acquired on the clean Ni surface (solid line) and after Pd deposition (dashed line) are shown in Fig. 3. All the Ni $3p$ spectra taken on the different grains on the Pd-free surface have the same line shape and energy position. The Ni $3p$ peaks measured on a Pd-covered surface are also similar for different grains but appear to be shifted by 0.2 eV with respect to the clean surface spectrum. The width of the Ni $3p$ spectrum of the clean surface is somewhat larger, because part of the signal comes from the Ni bulk atoms, which emit photoelectrons with energy different from that of the surface atoms. For our very surface-sensitive experimental setup, where most of the signal comes from the top two layers, deposition of a submonolayer of Pd attenuates the emission from Ni surface atoms so that the Ni $3p$ feature is now due essentially to emission from bulk atoms. The broadening observed for a clean surface is then due to emission from both bulk and

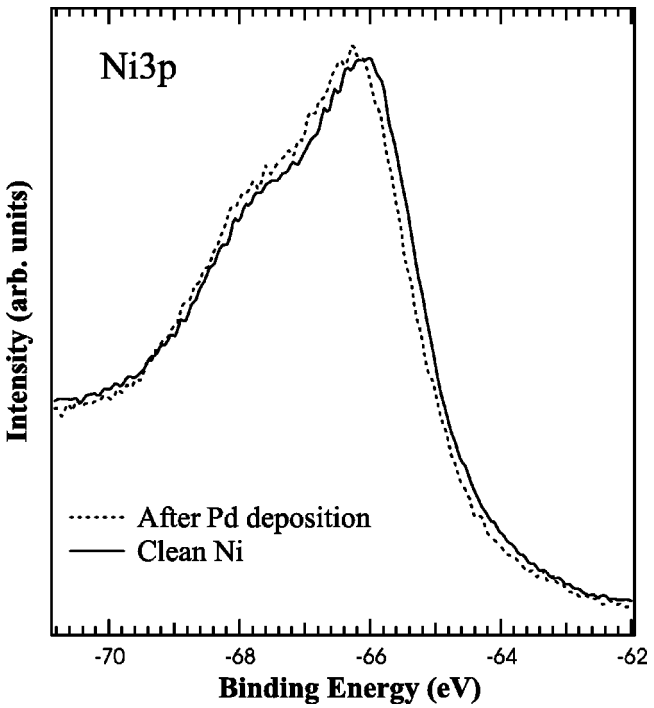

FIG. 3. The two Ni $3p$ core-level photoemission spectra shown correspond to the Ni sample before (solid line) and after the Pd deposition (dotted line). No differences have been found between the grains.

energy-shifted surface atoms. The binding energy shift of the Ni $3p$ spectra reflects the modification of the electronic structure of the surface Ni atoms resulting from changes in the atom environment produced by the presence of adsorbed Pd and Pd atoms embedded in the surface Ni layer, as discussed below.

Figure 4 shows several Pd $3d_{5/2}$ core-level spectra acquired on the different planes. The binding energies are determined with respect to the position of the Fermi level and the spectra are normalized in order to have the same intensity. It is clear from the line shape that all spectra contain more than one component. Good fits were obtained using Doniach-Sunjic functions convolved with Gaussians to include the instrumental broadening and other minor effects. The best fit corresponded to values of 0.5 eV for the Gaussian full width at half maximum (FWHM) for both features, an asymmetry of 0.1 and values for the Lorentzian FWHM of 0.2 eV for the low-binding-energy component, and 0.5 eV for the high-binding-energy component for all grains.

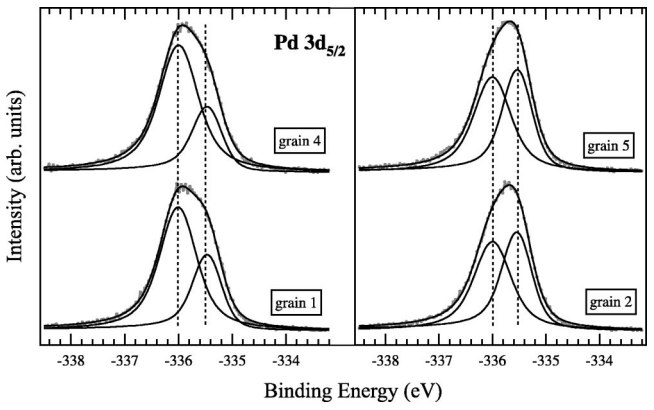

FIG. 4. Pd $3d_{5/2}$ photoemission spectra acquired on different Ni planes decomposed using two fitting components. The height of the peaks is normalized to the same value for clarity.

The fits of the spectra for all grains require the same two components centred at binding energies of 336.0 and 335.5 eV. The different degree of asymmetry of the spectra is simply due to the different intensity ratios between these two components, as can be seen in Fig. 4. It should be noted that the weight of the component at 336.0 eV is either dominant or comparable to the weight of the component at 335.5 eV. In order to assign the origin of the two components we refer to the reported Pd $3d_{5/2}$ binding energies of (i) pure bulk and surface Pd, 335.1–335.3 eV and 334.65–334.9 eV, respectively, for different Pd planes;[14–16] (ii) adsorbed single Pd atoms or small clusters of two to four Pd atoms, 336.4 to 336.0 eV (Ref. 17); and (iii) bulk and surface Pd in Pd_xNi_y alloys, 336.1 ± 0.1 eV and 335.4 eV, respectively.[6,8,18] The component at 336.0 eV can be assigned either to the bulk Pd in a Pd_xNi_y alloy or to the adsorbed Pd species. Since the experiments were performed at room temperature and the amount of Pd deposited was far below a monolayer, the formation of a bulk Pd-Ni alloy can be ruled out. This justifies the assignment of the component at 336.0 eV to an adsorbed Pd species, Pd_{ads} . For the present system the second component at 335.5 eV can then only be associated with Pd embedded in the top surface Ni layer, forming a surface alloy, Pd_{alloy} .

The multichannel detector energy window used for the Pd $3d_{5/2}$ photoemission images was chosen in order to have some channels at the energy positions of both components, Pd_{ads} and Pd_{alloy} , identified in the Pd $3d_{5/2}$ spectra. In this way maps corresponding to the lateral variations of each component could be obtained. Figures 5(a) and 5(b) show the Pd_{ads} and Pd_{alloy} maps, obtained after removal of the topographic contribution by dividing the image with a Ni image of the same area on a pixel-by-pixel basis, using the same procedure as for the Pd image in Fig. 2(c). The images reflect the relative concentration of the adsorbed and embedded Pd across the sample region. The signal is different between the grains but is mainly uniform within each grain. The Pd_{ads} signal is particularly intense on grain 1 and low on grains 2, 4, and 5 where the difference is negligible. The Pd_{alloy} signal seems to be uniform over all the grains except for grain 4. The pictures in Fig. 5(a) and 5(b) are displayed with the same gray-level scale so that the signals can be directly compared. Image 5(c) is the ratio between images 5(a) and 5(b) and illustrates the dominance of Pd_{ads} on grains 1 and 4, in accordance with the decomposed Pd $3d_{5/2}$ spectra shown in Fig. 4. From the gray levels of the maps in Fig. 5 and the decomposed Pd $3d_{5/2}$ spectra in Fig. 4, distribution plots of the total Pd amount, the Pd_{ads} species, and Pd_{alloy} species were obtained for the oriented grains 1, 2, and 5, and shown in Fig. 5(d).

C. Discussion

The present SPEM results on the interaction of Pd with the different grains of a polycrystalline Ni surface at RT are

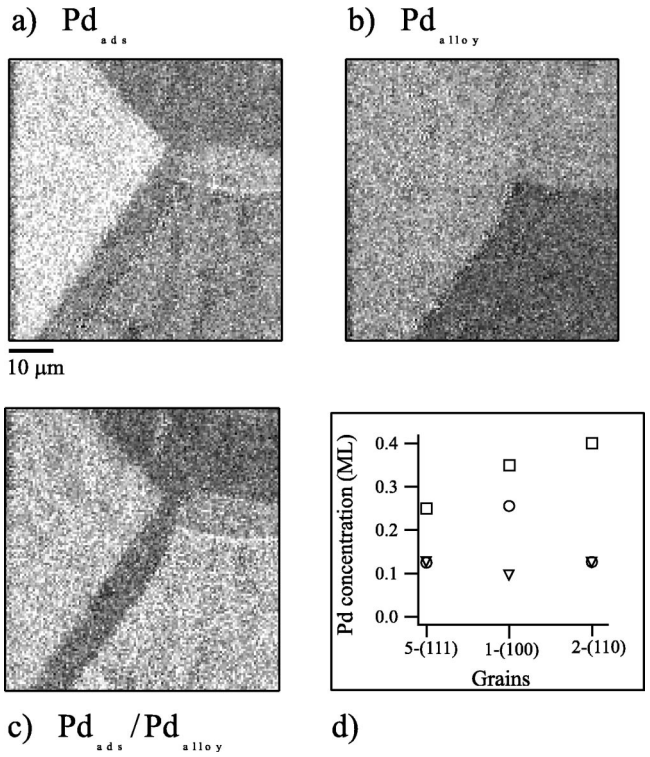

FIG. 5. (a) and (b) Chemical maps of the Pd_{ads} and Pd_{alloy} components illustrating the lateral distribution of adsorbed and embedded Pd between the grains. (c) A map, obtained by division of Pd_{ads} image by the Pd_{alloy} image on a pixel-by-pixel basis, illustrating the relative local concentration of adsorbed and embedded Pd. (d) A plot of the distribution of total (□), adsorbed (○), and embedded (▽) Pd between the grains with more ordered structure. The Pd concentration is expressed in ML with respect to the suggested local Ni surface concentration.

in excellent agreement with the STM study of the Pd/Ni(110) interface.[3,10,11] The microspot spectra and chemical mapping confirm the coexistence of two types of Pd species, adsorbed Pd and Pd embedded in the Ni surface lattice. However, our results clearly show considerable differences in the local surface concentration of Pd and in the extent of the surface Pd-Ni alloying on the different grains.

In order to explain our results we assume that the Pd atoms incident on the surface from the evaporator possess substantial mobility before being trapped in the equilibrium state. Typically evaporated metal atoms, as in the present case, carry a kinetic energy of order of 0.25 eV and gain additional adsorption energy, which is of the order of the heat of condensation, i.e., up to 4 eV,[19,20] by landing on the surface. The initially ''hot'' Pd atoms are then able to diffuse across the polycrystalline Ni surface for a sufficient time before equilibration. This gives uniform local grain coverage but with a different amount of adsorbed and embedded Pd on the different grains. The inhomogeneous Pd distribution between the grains means that the potential energy minima for adsorbed and embedded Pd depend upon the local structure of the grains.

Detailed inspection of the results illustrated in Figs. 4 and 5 leads to the following conclusions. The apparently regular grain 1 surface is the energetically most favorable for Pd adsorption, whereas the potential energy minima for surface alloying seem very similar for all grains except grain 4 (see Fig. 5). In fact, the disordered rough grain 4 appears to be the least favorable area both for Pd adsorption and surface alloying. This is contrary to the normal expectation that adsorption will be facilitated by the presence of steps and defects. One must, however, consider that since grain 4 is rather rough, it should also contain defect areas that might serve as local channels for vertical diffusion of Pd deeper into the bulk. A natural result of such in-bulk Pd diffusion would be a low Pd photoemission signal, particularly for the very small escape depth of the Pd $3d$ photoelectrons in our experimental setup. Our results cannot unambiguously rule out the possibility that the presence of low-energy barriers have facilitated vertical diffusion of Pd on grain 4. However, simple thermodynamic considerations concerning the lower surface tension and larger size of Pd with respect to Ni, which explain the observed large surface enrichment of Pd in PdNi alloys, suggest that defect-mediated Pd in-diffusion at room temperature is unlikely to be dominant on grain 4. The relative activity of the grains with respect to adsorption and alloying suggests that adsorption is a dominant process not only on ordered grain 1, but also for the disordered grain 4. On the other hand, the alloying and adsorption take place with equal probability on grains 2 and 5.

IV. CONCLUSION

In conclusion, the lateral distribution of a submonolayer coverage of Pd between the different grains of a polycrystalline Ni surface, the surface structures of which have been suggested by means of a LEEM and μ-LEED study, has been determined by combined chemical imaging and microspot photoelectron spectroscopy. The microspot Pd $3d_{5/2}$ spectra reveal the presence of two different Pd surface species, adsorbed on and embedded in the surface lattice of the grains. The local concentration of these two types of Pd species clearly depends on the structure of the crystal grain and on its detailed topography. For the present Pd/Ni system the mobility of the deposited hot Pd atoms appears to be rapid enough for the lateral distribution of Pd to follow the thermodynamic potential energy, which varies with grain structure. These results confirm the crucial importance of the surface morphology of metal films for the control of their local properties. This result is relevant to the many applications of polycrystalline materials, from catalysis to microelectronic and magnetic devices.

Further studies probing the development of the local composition of the Pd film during annealing are planned.

ACKNOWLEDGMENTS

We are grateful to Sincrotrone Trieste SCpA for allowing us access to the facility and providing support. The work was supported by an EC grant as Project No. 2000087.

[1] A. Bukaluk, Appl. Surf. Sci. **144-145**, 395 (1999).
[2] J. Tersoff, Phys. Rev. Lett. **74**, 434 (1995).
[3] L. P. Nielsen, I. Stensgaard, F. Besenbacher, and E. Laegsgaard, Surf. Rev. Lett. **3**, 1713 (1996).
[4] N. T. Barrett, R. Belkhou, J. Thiele, and C. Guillot, Surf. Sci. **331-333**, 776 (1995).
[5] N. T. Barrett, B. Villette, A. Senhaji, C. Guillot, R. Belkhou, G. Treglia, and B. Legrand, Surf. Sci. **286**, 150 (1993).
[6] P. Hermann, J. M. Guigner, B. Tardy, Y. Jugnet, D. Simon, and J. Bertolini, J. Catal. **163**, 169 (1996).
[7] M. Abel, Y. Robach, J.-C. Bertolini, and L. Porte, Surf. Sci. **454-456**, 1 (2000).
[8] J. Bertolin, P. Miegge, P. Hermann, J. L. Rousset, and B. Tardi, Surf. Sci. **331-333**, 651 (1995).
[9] L. Porte, M. Phaner-Goutorbe, J. M. Guigner, and J. Bertolini, Surf. Sci. **424**, 262 (1999).
[10] L. P. Nielsen, F. Besenbacher, I. Steensgaard, E. Laegsgaard, C. Engdahl, P. Stoltze, K. W. Jacobsen, and J. K. Nrskov, Phys. Rev. Lett. **71**, 754 (1993).
[11] U. Lipphardt, H. Engelhard, J. Westhof, and A. Goldmann, Surf. Sci. **294**, 84 (1993).
[12] M. Marsi, L. Casalis, L. Gregoratt, S. Gunther, A. Kolmakov, J. Kovac, D. Lonza, and M. Kiskinova, J. Electron Spectrosc. Relat. Phenom. **84**, 73 (1997).
[13] E. Bauer, J. Electron Spectrosc. Relat. Phenom. **114-116**, 975 (2000).
[14] S. Surnev, M. Sock, M. G. Ramsey, F. P. Netzer, M. Wilklund, M. Borg, and J. N. Andersen, Surf. Sci. **470**, 171 (2000).
[15] J. N. Andersen, O. Bjorneholm, A. Sandell, R. Nyholm, J. Forsell, L. Thanell, A. Nilsson, and N. Martensson, Synchrotron Radiat. News **4**, 15 (1991).
[16] A. Baraldi, S. Lizzit, M. G. Ramsey, and F. P. Netzer, Surf. Sci. **416**, 214 (1998).
[17] M. G. Mason, Phys. Rev. B **27**, 748 (1983).
[18] P. Miegge, J. L. Rousset, B. Tardy, J. Massardier, and J. Bertolini, J. Catal. **149**, 404 (1994).
[19] C. Smithells, *Metals Reference Book*, 2nd ed. (Interscience, New York, 1955), Vol. 2, p. 575.
[20] S. Chang and P. Thiel, Crit. Rev. Surf. Chem. **3**, 239 (1994).